Oppositely charged surfactants and nanoparticles at the air-water interface: Influence of surfactant to nanoparticle ratio

Eftekhari, M.; Schwarzenberger, K.; Karakashev, S. I.; Grozev, N. A.; Eckert, K.;

Originally published:

October 2023

Journal of Colloid and Interface Science 653(2024), 1388-1401

DOI: https://doi.org/10.1016/j.jcis.2023.09.038

Perma-Link to Publication Repository of HZDR:

https://www.hzdr.de/publications/Publ-37689

Oppositely charged surfactants and nanoparticles at the air-water interface: Influence of surfactant to nanoparticle ratio

Milad Eftekhari[a,b,*], Karin Schwarzenberger[a,b], Stoyan Ivanov Karakashev[c], Nikolay A. Grozev[c], Kerstin Eckert[a,b]

[a] *Institute of Fluid Dynamics, Helmholtz-Zentrum Dresden-Rossendorf, Dresden, Germany*
[b] *Institute of Process Engineering and Environmental Technology, Technische Universität Dresden, Germany*
[c] *Department of Physical Chemistry, Sofia University, Sofia, Bulgaria*

Abstract

Hypothesis: The interactions between oppositely charged nanoparticles and surfactants can significantly influence the interfacial properties of the system. Traditionally, in the study of such systems, the nanoparticle concentration is varied while the surfactant concentration is kept constant, or vice versa. However, we believe that a defined variation of both components' concentration is necessary to accurately assess their effects on the interfacial properties of the system. We argue that the effect of nanoparticle-surfactant complexes can only be properly evaluated by keeping the surfactant to nanoparticle ratio constant.

Experiments: Zeta potential, dynamic light scattering, high amplitude surface pressure and surface tension measurements are employed synergistically to characterize the interfacial properties of the nanoparticle-surfactant system. Interferometric experiments are performed to highlight the effect of surface concentration on the stability of thin liquid films.

Findings: The interfacial properties of surfactant/nanoparticle mixtures are primarily determined by the surfactant/nanoparticle ratio. Below a certain ratio, free surfactant molecules are removed from the solution by the formation of surfactant-nanoparticle complexes. Surprisingly, even though the concentration and hydrophobicity of these complexes do not seem to have a noticeable impact on the surface tension, they do significantly affect the rheological properties of the interface. Above this ratio, free surfactant monomers and nanoparticle-surfactant complexes coexist and can co-adsorb at the interface, changing both the interfacial tension and the interfacial rheology, and thus, for example, the foamability and foam stability of the system.

Keywords: `Nanoparticle surfactant complexes, Surfactant to nanoparticle ratio, Surface pressure isotherm, Zeta potential, Film stability`

1. Introduction

Particles play a critical role in numerous industrial applications [1–3], necessitating a comprehensive understanding of their behavior for proper process design in these domains. In certain industries, such as pharmaceuticals and food, particles are specifically designed and added to the system to improve product quality

*Corresponding author
Email address: `m.eftekhari@hzdr.de` (Milad Eftekhari)

and achieve desired properties [4–6]. Whereas in industries such as petroleum and agriculture, particles are naturally present and can have a significant impact on the underlying processes. For instance, in the petroleum industry, particles can increase the stability of unwanted emulsions, which can lead to an increase in pipeline pressure drop [7].

Most of the particles found in natural processes are not inherently surface active, yet their presence in a system containing surfactant molecules can greatly affect the interfacial properties of the system. The interaction between the two components is highly dependent on the characteristics of both the particles and the surfactants [8, 9]. Numerous studies have investigated the interactions between oppositely charged nanoparticles (NPs) and surfactants, as the formation of nanoparticle (NP)-surfactant complexes (NPSCs) is expected via electrostatic attraction forces [10–15]. The formed complexes are surface active and can adsorb at the interface [16]. The adsorption of surface active materials, whether in the form of particles or surfactant molecules, can reduce the interfacial tension and thus facilitate the formation of multiphase systems. Simultaneously, it enables interfaces to resist deformation and stress, thus stabilizing them [17–19].

The stabilizing effect of particles is a multifaceted process governed by several mechanisms. Particles can form a self-assembled rigid layer that provides stability through steric effects [20]. Moreover, their influence on the stability of the system extends to the alteration of the rheological properties at the interfaces, which manifests itself in effects such as variations in the film drainage rate [20, 21]. Various approaches have been used to investigate the stabilizing effect of different particles. One such approach is to study the response of interfacial layers to deformation under high amplitude compression, which can also provide valuable insight into particle interactions at the interface [22, 23]. Another approach is to directly study the stability of particle-laden interfaces. This can be accomplished by using a dynamic foam/emulsion analyzer [24, 25] to observe the entire foam/emulsion system, or by using interferometry to study the thinning behavior of a single film in the presence of particles [26, 27].

Despite the numerous studies that have addressed the behavior of oppositely charged NPs and surfactants, there is still no unanimous conclusion regarding the effects of NPSCs on the interfacial properties of the system. For example, while Ravera et al. [28] state that the addition of silica NPs increases the surface tension of the surfactant solution, Vatanparast et al. [22] argue that the presence of NPs further reduces the surface tension of the system. Furthermore, the crucial factors that dictate the surface pressure response of the particle-laden interface during compression have not been definitively identified [23, 29–31]. These factors are essential because they are directly related to the stability of multiphase systems.

In an attempt to connect the previous studies and to understand the effects of NPs on the interfacial properties of the system, we have performed profile analysis tensiometry (PAT) studies using silica NPs in the presence of the cationic surfactant Hexadecyltrimethylammonium bromide (CTAB) at the air-water interface. We consider the effect of particle size and concentration on the surface tension of the aqueous system for a wide range of surfactant concentrations. Remarkably, we introduce a novel perspective by analyzing the surface tension of these complexes in conjunction with results from zeta potential and dynamic light scattering measurements. This novel approach allows us to systematically identify the "critical ratio", i.e. the ratio of surfactants to

nanoparticles, at which all the introduced surfactants are adsorbed on the surface of the nanoparticles. Furthermore, we analyze the behavior of particle-laden interfaces under high amplitude compression while maintaining a constant surfactant/nanoparticle ratio. These analyses illustrate how particle concentration and hydrophobicity affect interfacial rheology, although their influence on surface tension remains minimal. Interferometric experiments are performed on specific systems to study the stability of thin liquid films in the presence of adsorbed NPSCs, emphasizing their significant role in maintaining the stability of multiphase systems. The results indicate that neither the concentration of surfactants nor the concentration of NPs alone determines the surface tension of the system. Unambiguous trends can only be obtained when the NP/surfactant ratio is kept constant.

2. Materials and Methods

2.1. Materials

CTAB (purity $\geq 99\%$, Merck) is used as the cationic surfactant. CTAB has a molecular weight of $364.45\,\mathrm{g\,mol^{-1}}$, a hydrophilic-lipophilic balance (HLB) of 10, and a critical micelle concentration (CMC) of 0.91 mM [32]. A commercial colloidal dispersion of silica NPs, Levasil 300/30 (with stock concentration of 30 wt.% Nouryon, Germany) and Ludox TM50 (with stock concentration of 50 wt.%Grace, US), were used as stock nanoparticle dispersion. The nominal particle sizes of the Levasil and Ludox dispersions used are 9 and 25 nm, respectively. Ultrapure water (from a Milli-Q ELGA apparatus, United Kingdom) with $18.2\,\Omega$ resistivity and organic content ≤ 2 ppb is used to prepare the aqueous solutions.

The surfactant concentrations in this study are denoted by x CMC, which indicates the relative concentration of the surfactant with respect to its CMC, e.g., 0.45 mM CTAB is designated as 0.5 CMC CTAB. Note that the addition of NPs may change the CMC of the system; however, whenever the CMC is referred to in the text, it is the CMC of CTAB in deionized water. The NPs are denoted as NP^{y}, where y indicates the average nominal diameter of the particles, e.g., NP^{25} means NPs of diameter 25 nm.

2.2. Sample preparation

The surfactant-nanoparticle dispersion samples were prepared by adding a specified amount of CTAB solution into the pre-diluted NP dispersion to obtain the desired concentrations. For example, to attain the desired composition of x CMC CTAB + y wt.% NP, the $2x$ CMC CTAB solution is added drop by drop to the $2y$ wt.% NP dispersion. The dispersion is prepared beforehand by diluting the original NP source concentration by adding the required amount of deionized water. The whole dispersion was continuously stirred during the drop-wise addition to avoid particle aggregation [14]. The final sample of the surfactant-nanoparticle dispersion was sonicated in an ultrasonic bath for at least 20 minutes. The temperature of the bath was controlled to avoid any destabilization or degradation within the system [33].

2.3. Zeta potential and dynamic light scattering (DLS)

Zeta potential and DLS measurements (reported as Lognormal Median Diameter by Intensity, also known as effective diameter) for NP solutions were performed using a NanoBrook 90Plus Zeta device (Brookhaven Instruments, USA). The experiments are carried out at 25°C including a 180 s delay after a steady device temperature has been reached in order to ensure the absence of temperature gradients within the sample. The samples were prepared by diluting the original dispersion with ultrapure water for DLS and zeta potential measurements [33]. It should be noted that this dilution changes the pH and ionic content of the system. The pH of the stock solution of Levasil 300/30 was 10 and LUDOX TM-50 was 9 as reported by the manufacturer.

2.4. Surface tension measurements

Profile analysis tensiometry (PAT-1M, Sinterface Technology, Germany) was used to evaluate the dynamic interfacial tension and surface pressure of the air-water interface. Thereby, the shape profile of the pendant drop, defined by the interplay of gravity and interfacial tension, is fitted to the Young-Laplace equation (YL), yielding the interfacial tension [34]. To understand the properties of the adsorbed layer of NPSCs, four cycles of large amplitude compression/expansion experiments were performed after the system reached equilibrium (see also SI, Fig. A.1a). The droplet surface area was gradually decreased and then increased back to the initial surface area. During this process, the change in interfacial tension was recorded. The corresponding surface pressure (see also SI, Fig. A.1b) was evaluated as the difference between the equilibrium interfacial tension of the uncompressed system and the interfacial tension under compression ($\Pi = \gamma_{eq} - \gamma$) as a function of the normalized surface area (A/A_0).

2.5. Interferometry measurements

Interferometry is used to study the thinning behavior of liquid films with adsorbed NPSC under controlled conditions. The method uses the interference of light waves to determine the thickness of a thin film by analyzing the resulting fringe pattern [35]. The apparatus comprises two basic units: the measuring cell ("Scheludko-Exerowa cell", Fig. 1a) in which the film is formed, and the optical-electronic system for monitoring the film and its thickness (Fig. 1b).

To form a film, the cylindrical part of the cell is first filled by dipping the film holder into the suspension and drawing in the solution. A double concave droplet is then formed by gently withdrawing liquid from the capillary outlet with a microsyringe, marked by the arrow in Fig. 1a. After the formation of the double concave droplet, different aging times can be set for the particles to adsorb at the two interfaces formed. Gradual withdrawal of more liquid causes the two interfaces of the double concave droplet to approach each other, resulting in the formation of the liquid film. The liquid film begins to drain under the effect of capillary pressure and its thickness can be monitored. The film is vertically illuminated (see Fig. 1b) with coherent light generated by an inverted microscope (model IX51, Olympus). The light is then reflected from both surfaces of the film. This produces two phase-shifted beams of reflected light, which are collected by a photodetector and recorded as a time series of interferograms [36]. The software "Image J" is used for processing of the recorded

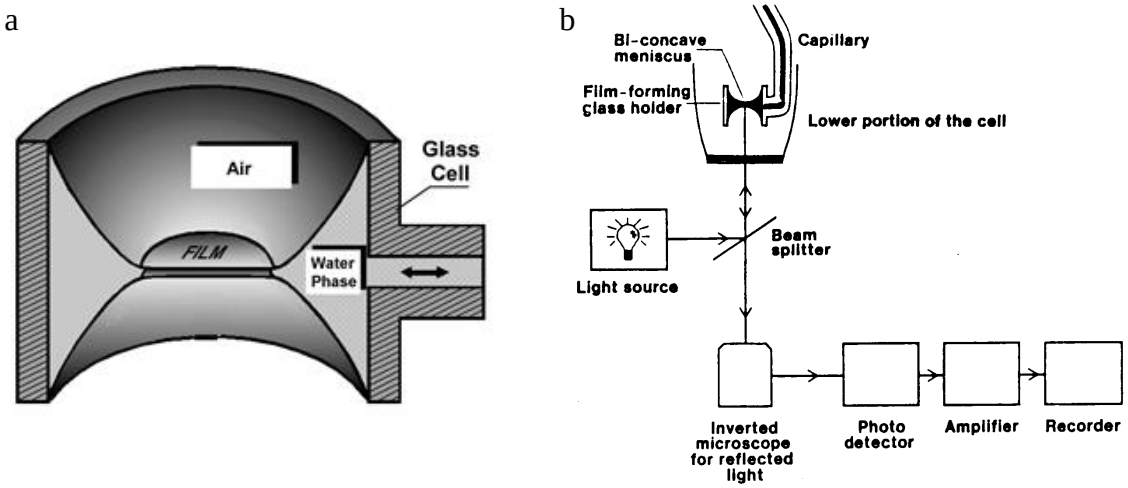

Figure 1: **a**) The Scheludko-Exerowa cell [36]. **b**) Experimental setup for studying thin liquid films [37].

images. The spatial interferogram of a frame shortly before film rupture was chosen for evaluation, which was considered appropriate to represent the characteristics of the liquid film. Once the spatial interferogram, i.e., image intensity along a selected line is extracted, the equation 1 is used to calculate the film thickness,

$$h = \frac{\lambda}{2\pi n_0}\left[l\pi \pm \arcsin\sqrt{\frac{\Delta(1+r)^2}{(1-r)^2+4r\Delta}}\right] \tag{1}$$

where λ is the wavelength of the monochromatic light after digital filtration (for green light $\lambda = 547\,\mathrm{nm}$), l is the order of interference, $\Delta = (I - I_{min})/(I_{max} - I_{min})$, I is the spatially varying pixel intensity, I_{max} and I_{min} are its maximal and minimal values, $r = (n_0 - n_1)^2/(n_0 + n_1)^2$ is the Fresnel reflection coefficient and n_0 and n_1 are the refractive index of water and air at T=20°C, respectively. The minimum signal for the film is usually taken from the signal of a ruptured film, while the maximum signal is taken from the digital interferogram. However, this does not apply to complex interferograms of films with very inhomogeneous thickness where the order of the interference is 2 and more. In these cases, multiple minimal signals I_{min} depending on the thickness of the film can be expected. Therefore, the analyses are performed with local I_{min} taken from the interferograms.

3. Results and Discussion

3.1. Effect of nanoparticles on surface tension of CTAB solution

The surface tension of the silica NP dispersion was measured for approximately 2000 s. The addition of NPs was found to have no significant impact on the surface tension of pure water at all NP concentrations and sizes, see Fig. A.2a for NP^9 and Fig. A.2b for NP^{25} in the SI. This proves that, first, the system is free of impurities and, second, the NPs are not surface active.

Fig. 2 shows the equilibrium surface tension values of nanoparticle-surfactant mixtures as a function of surfactant concentration for different NP sizes and concentrations. The addition of NPs increases the surface tension of the surfactant solution over almost the entire range of surfactant concentrations used in this study, regardless of the size and concentration of the NPs. The formation of nanoparticle-surfactant complexes (NPSCs)

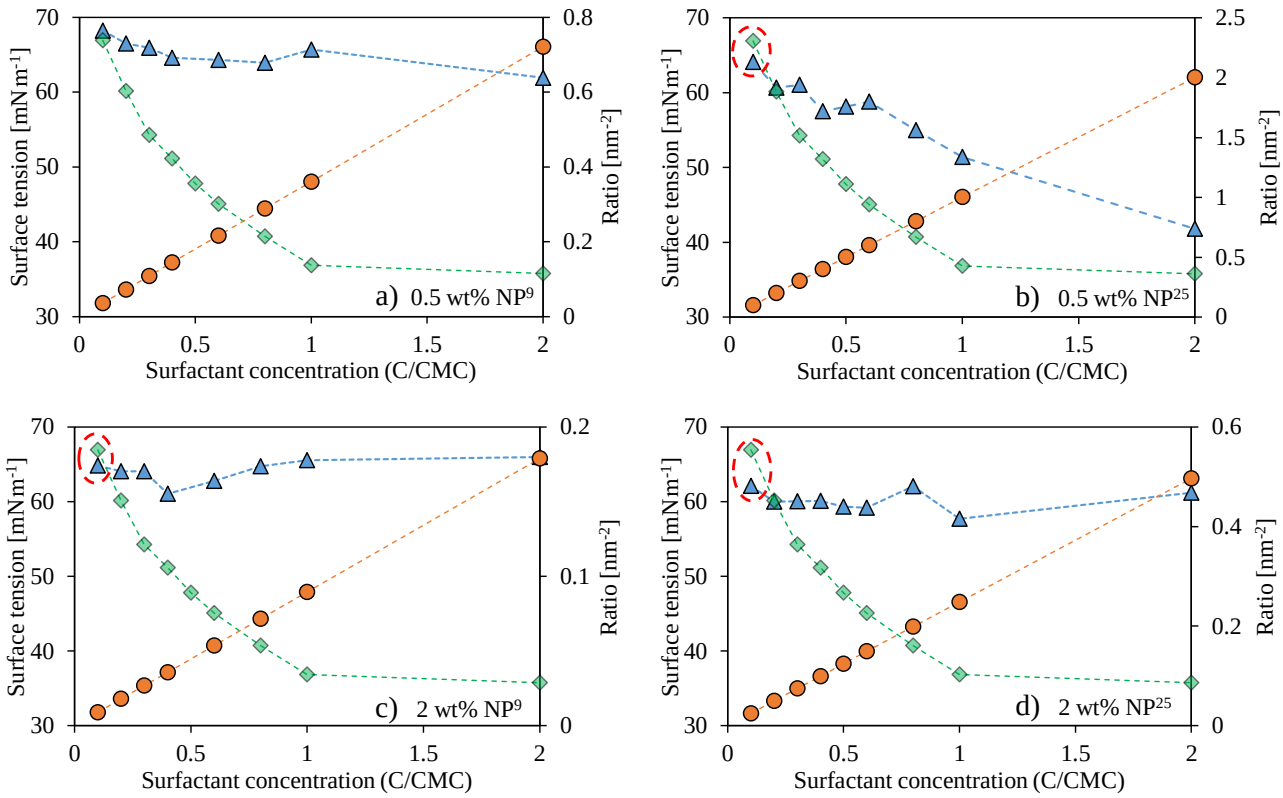

Figure 2: Equilibrium surface tension (filled blue triangles) vs. CTAB concentration for **a**) 0.5 wt.% 9 nm nanoparticles, **b**) 0.5 wt.% 25 nm nanoparticles, **c**) 2.0 wt.% 9 nm nanoparticles and **d**) 2.0 wt.% 25 nm nanoparticles. The green diamonds representing the reference surface tension of pure CTAB are plotted for comparison of the studied systems. The orange circles represent surfactant to nanoparticle ratios.

reduces the concentration of free surfactant molecules in the solution, and since the surface activity of NPSCs is significantly lower than that of surfactants [28], the surface tension of the system increases. It is only at very low concentrations of CTAB (around 0.1 CMC) that the addition of NPs reduces the surface tension of the surfactant solution, see the encircled points in Fig. 2. This means that even such a low concentration of surfactant can change the hydrophobicity of the NPs, leading to their surface adsorption and a slight reduction in surface tension. However, such a low concentration is not sufficient to significantly change the surface tension of pure water. The formed NPSCs under these conditions have a greater effect on surface tension considering their concentration and surface activity.

Furthermore, the results show that the surface tension of the mixtures containing NP^9 does not change significantly with increasing surfactant concentration. This is evident from the nearly flat trend of the surface tension curve as a function of CTAB concentration as shown in Fig. 2 a and c. In contrast, for NP^{25}, different trends are observed depending on the concentration of the NPs. The surface tension of the system decreases with increasing surfactant concentration at 0.5 wt.%NP^{25}, whereas it remains constant at 2.0 wt.%NP^{25}. It can also be inferred that larger particles provide lower surface tensions for given CTAB/NP concentrations. The size effect is particularly enhanced at higher surfactant concentrations and/or lower NP concentrations, see Fig.

A.3 in the Supporting Information for a better illustration of the size effect.

Fig. 2 also shows the number of surfactant molecules per unit area of the NPs [nm^2], simply referred to as the surfactant/NP ratio [nm^{-2}], versus surfactant concentration. The ratio is calculated as the ratio of added surfactants to added NPs. The results indicate that the surface tension remains relatively constant with increasing surfactant concentration, provided that the surfactant/NP ratio is below 0.6 nm^{-2}. In contrast, for ratios above 0.8 nm^{-2}, as shown in Fig. 2b, a significant decrease in surface tension with increasing surfactant concentration is observed.

3.2. Zeta potential and dynamic light scattering

Fig.3 shows the results of zeta potential and DLS measurements for 0.5 wt.% of NP^{25} and NP^{9} with different concentrations of CTAB. Initially, the magnitude of the zeta potential decreases with increasing surfactant concentration. However, at a certain concentration of surfactant, the exact value of which depends on the size and concentration of the NPs, the system reaches its isoelectric point (IEP). Beyond this point, the sign of the zeta potential changes and increases as the surfactant concentration increases. The system reaches its IEP at roughly 0.73 CMC for NP^{25} and about 1.8 CMC for NP^{9}. The change in sign of the zeta potential

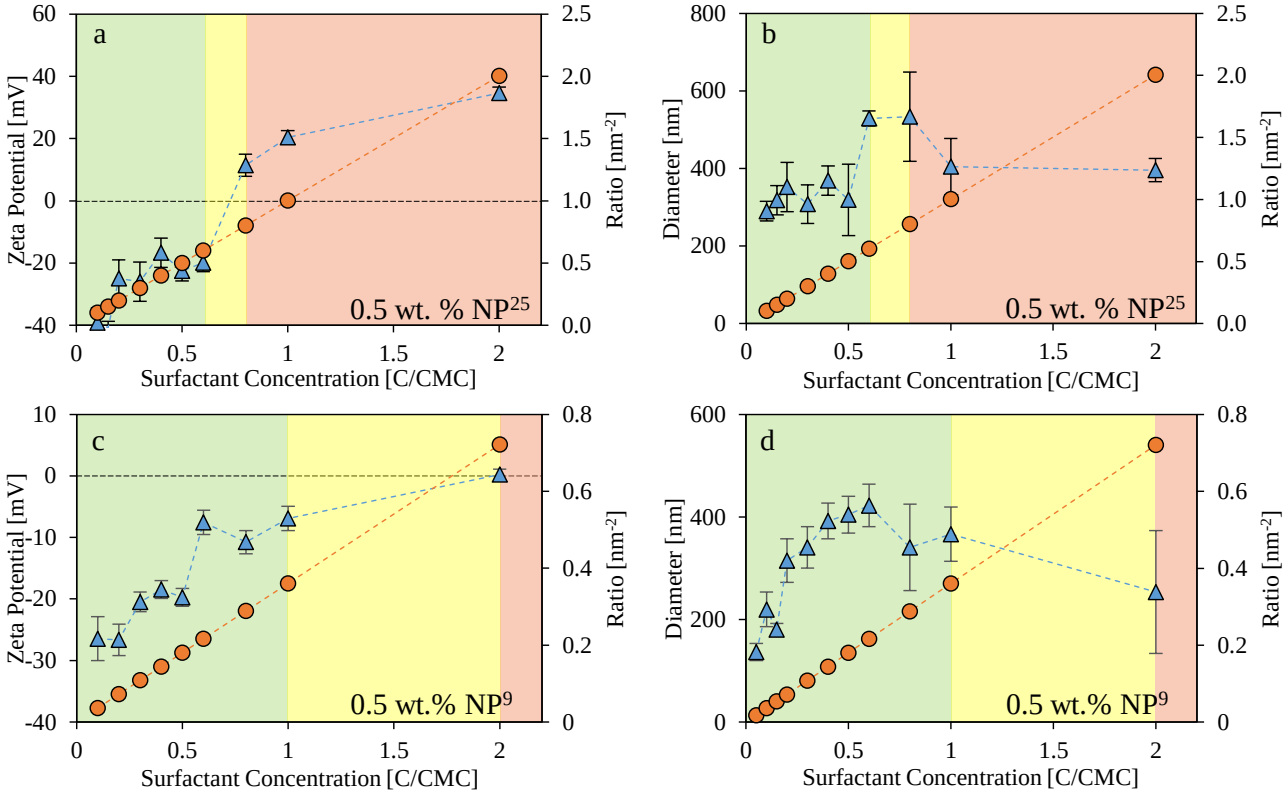

Figure 3: Zeta potential (**a** and **c**, blue triangles) and effective diameter (**b** and **d**, blue triangles) results vs. surfactant concentration for NP^{25} (**a** and **b**), and for NP^{9} (**c** and **d**), respectively. The orange circles represent surfactant to nanoparticle ratios. The green area indicates the range of ratios below IEP, the red area corresponds to the range of ratios above IEP, and the yellow area indicates the transition range in which the IEP is located.

is due to the hydrophobic interaction of the non-polar tails of the surfactant molecules. As the surfactant concentration increases, the surface charge decreases and the strong electrostatic forces diminish. Hence, the weaker hydrophobic forces gain influence, leading to the adsorption of the surfactant molecules in a reversed orientation on the particle surface, resulting in bilayer formation and a positive charge on the particles.

The dynamic light scattering results show clear indication of particle agglomeration, even at low surfactant concentrations. In particular, the average diameter of NP^9 shows a consistent increase with increasing surfactant concentration. On the other hand, for NP^{25}, the average diameter does not undergo substantial growth with surfactant concentration below the isoelectric point (IEP). However, as expected, a sharp increase in average diameter is observed near the IEP, followed by a subsequent decrease at higher surfactant concentrations. This decrease in average diameter suggests that the NPs are re-stabilized by the electrostatic repulsion generated by the positively charged surfactant bilayer formed on their surface. It is important to note that near the IEP, the sample shows a pronounced instability, mainly due to the reduction of the repulsive forces, which facilitates the agglomeration of the particles. This is evidenced by the two phases formed in the suspension. This tendency to agglomerate is further supported by the relatively high polydispersity index observed in DLS results for particle suspensions close to the IEP. Therefore, great care must be taken when interpreting and analyzing measurements under these circumstances.

3.3. Surface tension measurements at constant surfactant to nanoparticle ratio

As observed in Fig. 2, up to a certain surfactant/nanoparticle ratio (denoted as c^{crit} in Fig. 4a), the surface tension remains relatively constant with increasing surfactant concentration, meaning that all the added surfactant is adsorbed on the surface of the NPs [38, 39] and not at the air-water interface. Beyond this ratio, referred to in this study as the critical ratio, the surfactants begin to distribute between the aqueous phase (hence the air-water interface) and the surface of the NPs (see Fig. 4b) until the surface of the NPs reaches its maximum capacity (denoted as c^{Max} at Fig. 4d). Somewhere between c^{crit} and c^{Max}, the surfactant molecules begin to adsorb in the form of bilayers on the surface of the NPs and the zeta potential changes its sign, shown as c^{IEP} at Fig. 4c.

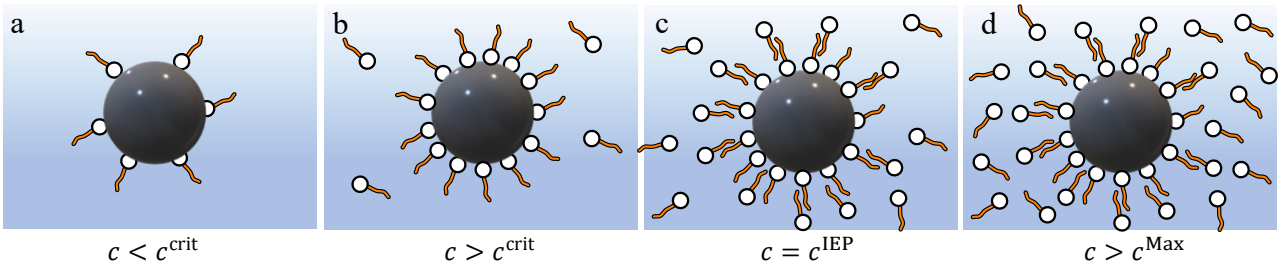

Figure 4: Schematic representation of surfactant adsorption on a particle surface.

Based on the results of the surface tension measurements, the critical ratio is expected to be in the range of $0.6\,\mathrm{nm}^{-2}$ to $0.8\,\mathrm{nm}^{-2}$. Considering that the isoelectric point is around the ratio of $0.74\,\mathrm{nm}^{-2}$, the surfactant/NP ratio range for the critical ratio can be further narrowed down to $0.6 \ldots 0.74\,\mathrm{nm}^{-2}$, since the critical ratio must

be lower than the isoelectric point ratio [39]. This approach is valid only if the zeta potential remains the same for different NPSC concentrations at the same ratio. Fig. A.4 in the SI shows that, indeed, the zeta potential remains relatively constant over different concentrations of NPSCs at the same ratio. Certainly, it's worth highlighting that the zeta potential does exhibit slight variability with NPSC concentration, primarily attributable to the influence of changes in ionic strength and pH resulting from the process of dilution.

The surface area of the CTAB molecule on the particle surface is calculated from these values to be about 1.4 nm^2 to 1.7 nm^2, assuming a monolayer surface coverage. The reported molecular cross sectional area of CTAB head groups at the water/air interface is approximately 0.4 nm^2-0.6 nm^2, measured by various techniques such as neutron reflectometry and Langmuir-Blodgett method [39, 40]. Since the calculated value is larger than the actual surface area of the CTAB, it can be concluded that the surfactant concentration on the particle surface is still quite sparse at the critical ratio. The maximum adsorption capacity (c^{Max}) of silica NPs in the study of Wang et al. [39] is found to be around 3.1 nm^{-2}, which expectedly is higher than the calculated critical ratio in this study.

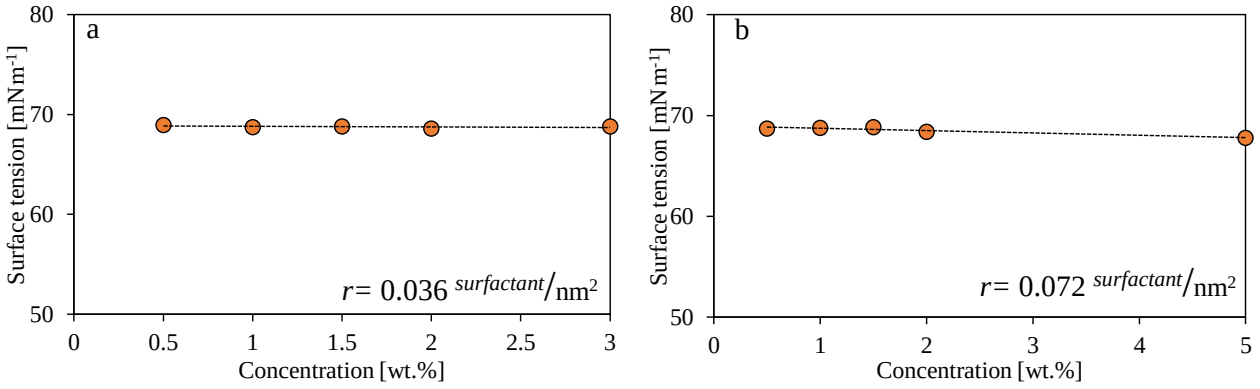

Figure 5: Equilibrium surface tension measurements of different concentrations of NPSCs solutions with constant ratio of adsorbed surfactant molecules per nanoparticle: **a**) 0.036 nm^{-2} and **b**) 0.072 nm^{-2}.

The effect of NPSCs concentration on the interfacial tension of the system is studied, while keeping the nature of the NPSCs constant. Fig. 5 a and b show surface tension as a function of NPSCs concentration at fixed surfactant to NP[9] ratios of 0.036 and 0.072 surfactant per nm^2, corresponding to 9 and 18 surfactant per nanoparticle, respectively. The ratios are selected according to three criteria: First, the systems have sufficient stability, since the surface charges are not completely neutralized, and second, they are among the most studied concentration ranges in the literature. And finally, both of these ratios are well below 0.5 nm^{-2}, which means that the surface tension is expected to remain constant. The concentration of NPSCs is calculated based on the concentration of nanoparticles added to the system. Evidently, at a constant surfactant/nanoparticle ratio, increasing the concentration of NPSCs has little to no effect on the surface tension of the system. The slight decrease in surface tension may be due to changes in the ionic strength and pH of the solution resulting from the increased NPSC concentration. These changes are expected to affect the behavior of the surface tension [9]. Collectively, it can be concluded that either the concentration of NPSCs has no significant effect on surface

tension, or even the lowest concentration is too high to capture the concentration dependence of surface tension.

3.4. Large amplitude compression/expansion experiments

The mechanical properties of particle-laden interfaces play a crucial role in stabilizing multiphase systems. The effective stabilization strongly depends on the rheological behavior of such monolayers, as in many industrial applications, the interfaces are subjected to large deformations that generate compressive and shear stresses [23]. Additionally, as recently reported [33], the hydrodynamic behavior of bubbles and droplets changes significantly under large amplitude compressions. Therefore, large amplitude compression/expansion cycles were performed to better understand the mechanical properties of the systems under study. After reaching equilibrium, the droplet volume was linearly reduced (about 80% of the initial droplet volume) and the changes in surface tension were evaluated. The compression/expansion cycles were repeated a total of 4 times at 150 s intervals (protocol shown in Fig.A.1 in SI).

To maintain brevity, this section will exclusively discuss the results related to the 0.036 nm^{-2} ratio and will focus solely on two concentrations. For additional concentrations, please refer to the SI (Fig. A.5), or for the higher ratio of 0.072 nm^{-2}, refer to the Fig. A.6. To investigate the hysteresis phenomenon, the surface pressure

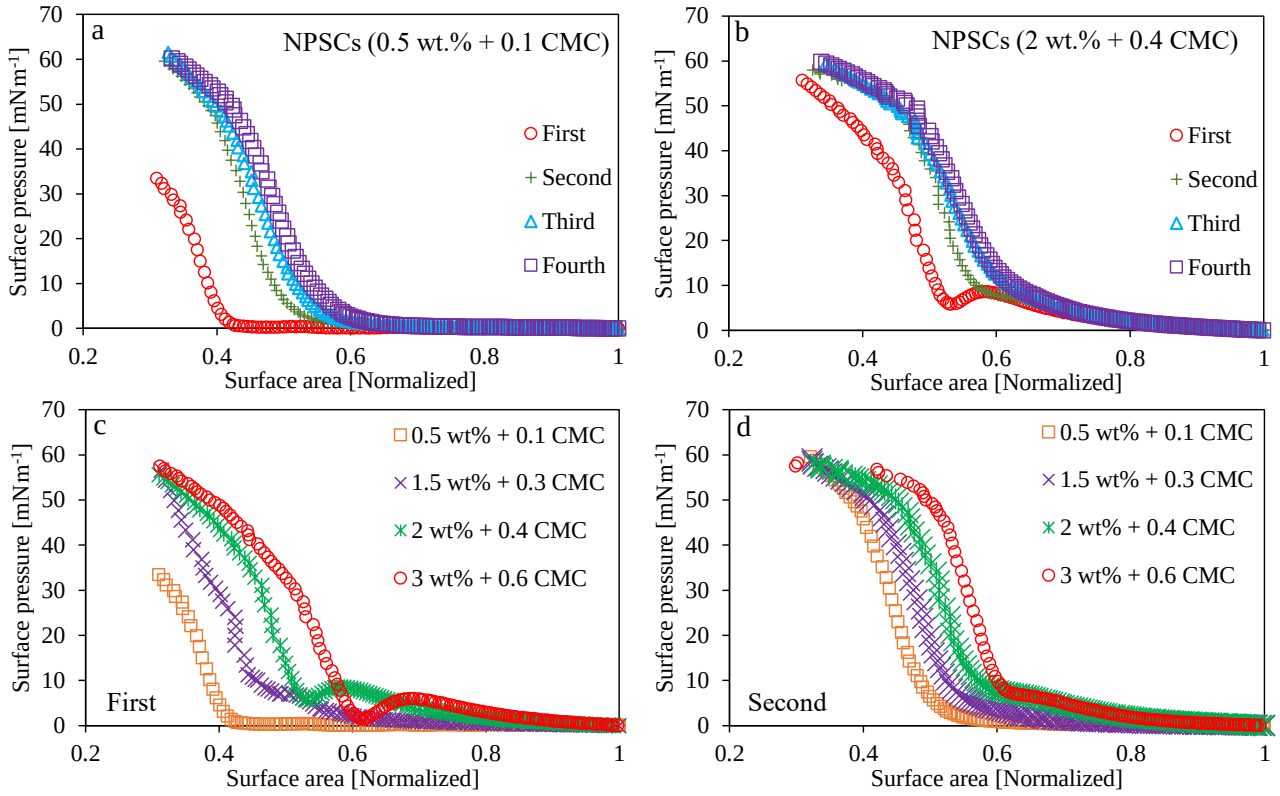

Figure 6: Surface pressure as a function of surface area for different compression cycles i.e., first, second, third, and fourth for **a**) 0.5 wt.% + 0.1 CMC CTAB and **b**) 2.0 wt.% + 0.4 CMC CTAB. Surface pressure as a function of surface area for different concentrations of nanoparticles and surfactants for **c**) first compression/expansion cycle **d**) second compression/expansion cycle. The ratio of surfactant to nanoparticles was 0.036 nm^{-2} for all figures.

isotherms of the different compression-expansion cycles are shown in Fig. 6 a and Fig. 6 b for 0.5 wt.% + 0.1 CMC and 2.0 wt.% + 0.4 CMC, respectively, at a fixed surfactant/nanoparticle ratio of 0.036 nm^{-2}. Regardless of the concentration (ranging from 0.5 wt.% to 2 wt.%) or the type of NPSC (0.036 nm^{-2} and 0.072 nm^{-2}), the surface pressure curve shows significant hysteresis and shifts consistently to the right with each cycle, indicating a comparable surface pressure at higher surface area. Notably, the shift is particularly pronounced from the first cycle and becomes less noticeable in subsequent cycles. Interestingly, the surface tension value at the beginning of each compression was very similar and close to the equilibrium surface tension. This indicates that performing the compression/expansion cycle did not significantly affect the surface tension value. It is known that after the first compression, the particles tend to stay together in the form of small clusters and maintain an interconnected network [23]. These formed clusters interact with each other during repeated compression and increase the surface pressure, which explains the shift of the isotherms after the first cycle. Each expansion creates a new surface area that can accommodate additional particles, which in turn leads to increased particle-particle interactions over larger surface areas, explaining the rightward shift of the isotherm from cycle 2 to 4. This might seem contradictory to the aforementioned similar surface tension prior each compression cycle. However, as shown in Fig. 5, the surface tension shows a very weak dependence on the surface concentration of the particles, assuming that the surface concentration changes with the bulk concentration.

The surface pressure isotherms of different concentrations of NPSCs at a fixed ratio of 0.036 nm^{-2} are plotted for the first and second cycles in Fig. 6 c and Fig. 6 d, respectively. In the Supporting Information, Fig. A.7 shows the third and fourth cycles at the previously mentioned ratio of 0.036 nm^{-2}, and Fig. A.8 shows corresponding experiments covering all four cycles at the constant ratio of 0.072 . The surface pressure isotherm shifts to the right with increasing NPSC concentration over all compression/expansion cycles at both surfactant/NP ratios. Since the hydrophobicity of the particles is kept the same in each figure, the effect can only be attributed to the number of particles in the solution, which can affect the number of particles at the interface. This means that the (quasi-)equilibrium surface tension is not a sufficient indicator of the NPSCs behavior, as it is almost identical for all NPSCs in the uncompressed state, as shown in Fig. 5.

To investigate the effect of particle hydrophobicity at a fixed NP concentration, the surface pressure isotherms for the two different hydrophobicities (surfactant/NP ratio 0.036 nm^{-2} and 0.072 nm^{-2}, respectively) are plotted side by side in Fig. A.9. The results show that increasing the hydrophobicity of the particles shifts the isotherm to the right, i.e. to higher surface areas, for 1.5 wt.% nanoparticles for all compression cycles.

3.5. Effect of aging time

In previous experiments, compression/expansion cycles were performed after reaching equilibrium. However, in practical scenarios, such a condition may not always be met. Thus, to explore the effect of drop age on the interface response to large amplitude surface perturbations, compression/expansion experiments are performed at extended time intervals namely 100, 500, 1000, and 2000 seconds after drop formation. An exemplary result for 0.5 wt.% + 0.3 CMC CTAB is shown in Fig. 7. Although the surface tension of the uncompressed droplet does not change much (see Fig. 7a), the response of the interface to large amplitude compression shows marked

differences between compressions performed at earlier and later stages (see Fig. 7b). The possible effect of previous cycles is also investigated by compressing different droplets of the same solution at corresponding times without previous compression, see Fig. 7a. The previous cycles do not significantly change the overall behavior, i.e., the longer the waiting time, the stronger the surface tension response.

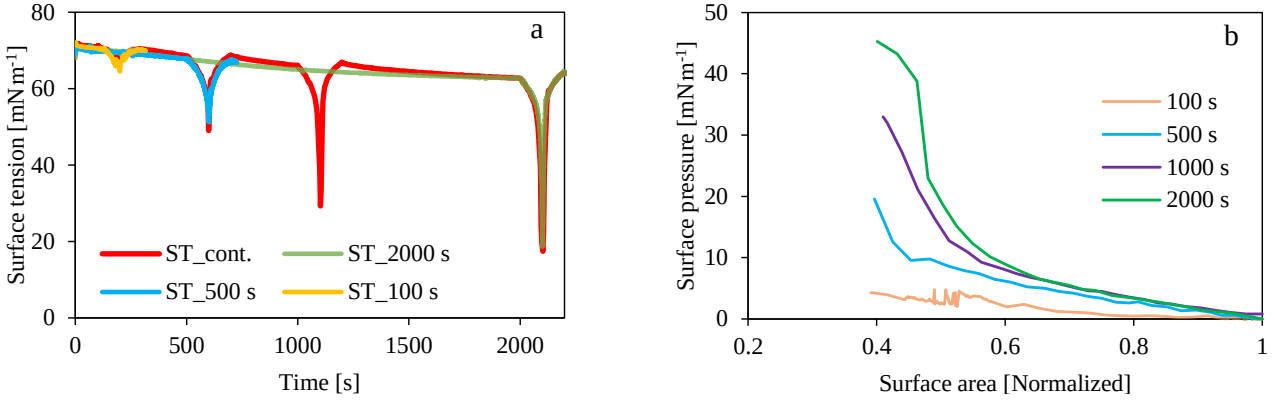

Figure 7: Effect of the onset time of compression/expansion on **a) the dynamic interfacial tension response** and **b) the surface pressure response** for 0.5 wt.% + 0.3 CMC CTAB.

To further emphasize the effect of aging time on the rheological behavior of the interfaces, and to directly demonstrate the technological relevance, the stability of thin liquid films stabilized with the NPSC system of 0.3 CMC CTAB + 2 wt.% silica NPs is studied for three different aging times: (i) immediately after formation of the double concave drop; (ii) 15 minutes after the formation of the double concave drop; (iii) 30 minutes after the formation of the double concave drop in the Scheludko-Exerowa cell, which are referred to as Type I, II, and III films, respectively.

It was observed that Type I liquid films are short living, i.e., they ruptured within seconds after their formation. Fig.8a presents a typical liquid film of Type I, obtained immediately after formation of the double concave drop. The film thickness strongly increases at the rim of the film, and a central dimple with larger film thickness (Fig.8b) can be observed in the center of the film, which frequently occurs during film drainage. However, in comparison with systems containing only surfactants, this is an unusual liquid film that exhibits sharp thickness inhomogeneities due to the presence of adsorbed NPSCs on the interface and presumably also in the liquid in the lamella. Type II liquid films have a significantly longer lifetime of approximately 6-7 seconds or more compared to Type I films. The rupture is initiated by the formation of an irregular hole that gradually expands over several seconds, as shown in Fig. A.10. The slow expansion is a remarkable indication of the significant surface viscosity imparted by the presence of NPSCs. The majority of the Type III liquid films had an extended lifetime of more than 30 minutes and were also characterized by inhomogeneous thickness, similar to the other types. In addition, an intriguing phenomenon of a slowly folding film surface was observed at the beginning of the rupture process (Fig. 8c), which is attributed to the solid-like state of the liquid film due to the adsorbed NPSC layer. Fig. 8d shows the film thickness profile on a selected line from the general interferogram in Fig. 8c, which shows significant thickness inhomogeneity varying from 200 nm to about 500 nm with abrupt

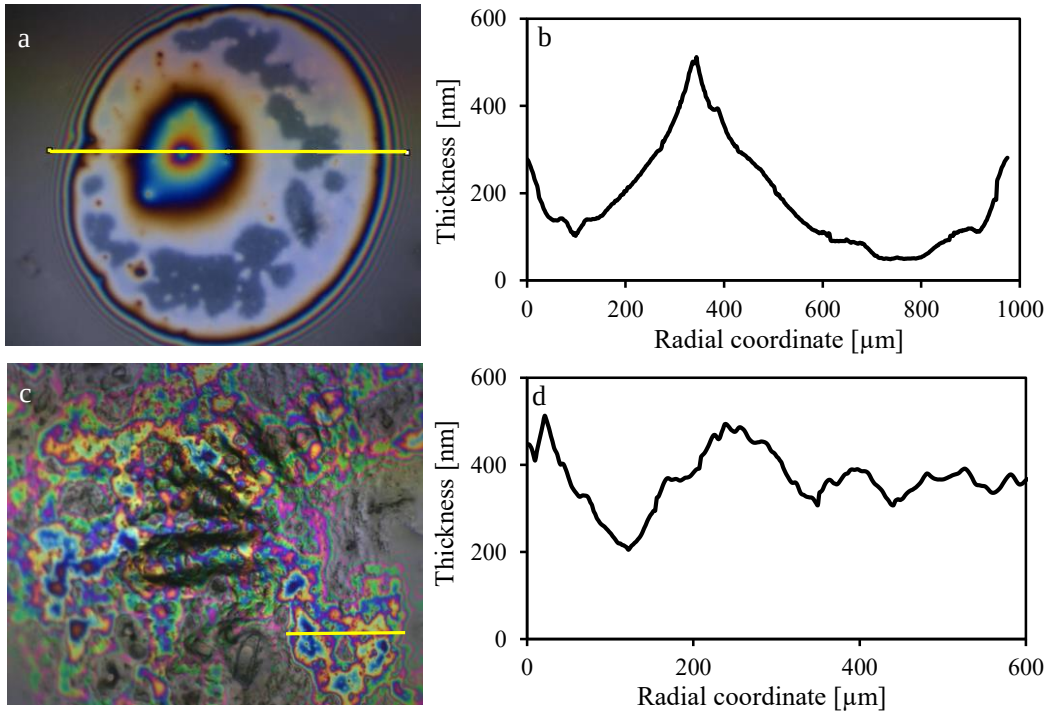

Figure 8: Interferogram of liquid film for **a**) Type I film and **c**) Type III film. Film thickness profile on the yellow line of the interferogram for **b**) Type I film and **d**) Type III film.

thickness changes along the profile. Considering the relatively small nominal size of the nanoparticles (9 nm), such a pronounced thickness inhomogeneity of the film is due to strong aggregation of the particles (around 300 nm), which are rather randomly distributed at the interface and presumably in the liquid in the lamella.

There are several mechanisms by which particles can affect the stability of thin films. Particles can increase the viscosity of the aqueous phase within the lamella, slowing liquid drainage [41]. They can also form a layered structure within the thinning film, leading to stabilization by oscillating structural forces that arise when spherical particles are confined between two surfaces [42]. The notable thickness inhomogeneity observed in Figure 8a indicates the presence of randomly distributed highly aggregated particles within the lamella. In the case of Type I films, it can be confidently stated that the particles have not had sufficient time to adsorb at the interface and are therefore predominantly within the liquid film. These aggregates can bridge adjacent bubbles and create a physical connection between the bubbles, allowing gas transfer between the bubbles and potentially destabilizing the film at thicker distances. However, particles bridging between bubbles in a foam can also form a network-like structure that strengthens the foam structure. The particle bridges act as physical barriers that prevent the thinning and breaking of liquid films between bubbles, thereby inhibiting coalescence. The ability of particles to stabilize the foam film through a bridging mechanism depends on several parameters, the most important of which are the hydrophobicity and shape of the particles.

In Type II and Type III films, particles are adsorbed at the interfaces and can therefore create a steric/mechanical barrier to coalescence. The presence of adsorbed particles can also alter the curvature of the gas-liquid interface,

reducing the pressure difference between the plateau borders and the associated films, ultimately increasing the stability of the thin film [6, 41]. If aggregate formation had led to film destabilization, one would expect to see more rapid destabilization with longer aging times. This is because the aggregates should expand and increase in size over time, contributing to the destabilization process. Since such a trend was not observed, it could be concluded that the particles, even considering the aggregates as a whole, should stabilize the interfaces and the stabilization effect outweighs the bridging effect. Nevertheless, the presence of aggregates should cause the film to rupture at thicker distances.

4. Discussion

Different trends can be observed when investigating the synergetic effect of oppositely charged nanoparticles and surfactants [22, 28]. Adding particles can increase or decrease the surface tension of the surfactant solution over a wide range of NP and surfactant concentrations. The results presented in the study show that neither the concentration of the surfactants nor the concentration of the nanoparticles alone can determine the surface tension of the system. More conclusive trends can only be obtained when considering the surfactant to NP ratio. We postulate that this principle holds true for materials where electrostatic attraction serves as the primary driving force for complex formation; see Fig. A.11 in the SI for similar experiments performed with DTAB, which has a shorter hydrocarbon tail.

Surface tension measurements show two distinct regions: below the critical surfactant/NP ratio, the surface tension remains constant with increasing surfactant concentration (Fig. 2). This region can be further divided into two sub-regions: at very low ratios, the inclusion of nanoparticles decreases the surface tension of the surfactant solution (see encircled points in Fig. 2), while at higher ratios, still below the critical ratio, the incorporation of nanoparticles increases the surface tension of the surfactant solution. Above the critical ratio, the surface tension values begin to decrease with increasing surfactant concentration (Fig. 2b). In this region, surfactant monomers and NPSCs coexist and can co-adsorb at the interface. This is demonstrated by combining high-amplitude compression (Fig. 7) and dynamic surface tension measurements(Fig. A.12). The former shows the presence of NPSCs at the interface as the interface collapses upon compression, while the latter shows a rapid decay of the surface tension, which is indicative of the adsorption of free surfactant molecules.

Our measurements indicate that NPSCs concentration and hydrophobicity have no significant effect on the equilibrium surface tension of the system as long as the surfactant to nanoparticle ratio remains below the critical ratio (5). However, increasing the hydrophobicity of NPSCs or their concentration can significantly change the rheological properties of the interface (Fig.6). For example, increasing the concentration/hydrophobicity of NPSCs causes the surface pressure isotherm to rise faster (see Fig. A.9 in the SI for hydrophobicity effect on surface pressure). This means that increasing the concentration/hydrophobicity of NPSCs either increases the number of the NPSCs at the interface or causes stronger inter-particle interactions at the interface. As the concentration/hydrophobicity of NPSCs increases, the tendency of the NPSCs to adsorb at the interface increases. It can also be argued that the more hydrophobic NPSCs have a lower surface charge, which reduces the electrostatic repulsion barrier for the adsorption of new NPSCs, resulting in more populated interfaces.

The faster increase in surface pressure for more hydrophobic NPSCs also might be affected by the higher steric hindrance of such NPSCs, which is caused by the chain length of the surfactant molecules adsorbed on the NPSCs, increasing the interparticle interactions. The CTAB molecule is 1.5 to 2 nm in length [43]. Given the nominal size of the particles, $D_p = 9\,\text{nm}$ less than 50 to 30 percent of the particles are needed compared to bare nanoparticles to achieve a similar packing density. For this estimation, the electrostatic interactions are ignored and the contact condition is assumed.

At a constant surfactant/nanoparticle ratio and below the critical ratio, increasing the concentration of NPSCs did not significantly change the surface tension of the system (5). Purely arithmethically (see below), even at the lowest concentration, there are enough particles in the system to completely occupy the interface. Since NPSCs adsorb irreversibly, their adsorption behavior is governed mainly by kinetic rather than thermodynamic factors. This means that the final state would be the same for different concentrations because the maximum amount of surface-active material that can be adsorbed on the surface is reached when the surface is completely covered, neglecting multi-layer adsorption. The percentage of nanoparticles at the interface relative to the total number of the nanoparticles added to the solution can be calculated using the following equation:

$$\%\text{of particle at the interface} = \frac{(A_d/V_d)(V_p/A_p)(\rho^p/\rho^w) \times \eta}{\chi}, \tag{2}$$

where V_d is the droplet volume and A_d is its surface area, V_p is the volume of the nanoparticles and A_p is their cross-sectional area, χ is the mass fraction of the nanoparticles, and η is the packing density of the nanoparticles at the interface. For a spherical droplet with a diameter of 3 mm and spherical nanoparticles with a diameter of 9 nm and χ as low as 0.25 wt.%, and assuming the highest interfacial packing density (η), i.e. 0.91, corresponding to hexagonal packing density, the percentage of nanoparticles at the completely covered interface will be less than 1 %. Even if the aggregated particle diameter of approximately 400 nm is included in the equation, the percentage of nanoparticles at the completely covered interface would be less than 1 %. This indicates that there are enough NPSCs available, even at 0.25 wt.% concentration of NPSCs, to fully cover the interface, which explains why the surface tension of NPSCs does not change significantly with the bulk concentration of NPSCs. Indeed, the surface concentration of the NPSCs also depends on the activity coefficient of the NPSCs and the magnitude of the adsorption barrier, both of which can change based on the bulk concentration of the NPSCs.

5. Conclusions

This research aims to extend previous findings [10–12, 14, 22, 28, 44–46] on the effect of oppositely charged surfactants and nanoparticles (NPs) on interfacial properties. To comprehensively address this overarching issue, the study covers the full parameter space, including different concentrations and sizes of silica NPs, along with different surfactant concentrations. Our results highlight the surfactant/NP ratio as the predominant influencing factor on the interfacial behavior of the system, outweighing the influence of both surfactant concentration and NP concentration.

A critical ratio, indicating the surfactant/NP ratio below which all added surfactant molecules are adsorbed on the NP surface, is introduced and experimentally measured by combining surface tension and zeta potential

measurements. The ratio ranges from $0.6\,\mathrm{nm}^{-2}$ to $0.74\,\mathrm{nm}^{-2}$ and agrees well with the values calculated from the data of Ravera et al. [28] and Wang et al. [39]. The surface tension of the system remains nearly constant for different surfactant and NP concentrations as long as the surfactant/NP ratio remains below this critical ratio. Conversely, the surface pressure isotherms showed a significant dependence on the concentration of nanoparticles and surfactants. Upon surpassing the critical ratio, the system accommodates both nanoparticle-surfactant complexes (NPSCs) and free surfactant molecules that can co-adsorb at the interface. Consequently, the surface tension of the system decreases as the surfactant concentration increases.

By increasing the concentration of NPSCs while maintaining a constant surfactant/NP ratio below the critical ratio, we observed that the surface tension of the system does not show significant changes with the concentration of NPSCs. In contrast, the surface pressure experiments showed a significant influence of the NPSC concentration. Similarly, time-dependent surface pressure experiments showed a significant change in the structure of the interface with time, while the interfacial tension showed a negligible change with time. Such changes in interfacial structure over time are also visualized by our film stability experiments.

Further work is needed to determine whether the surface concentration of these complexes increases or their interfacial structure changes with time or bulk concentration. The striking impact of the adsorbed particle layer on the film rupture dynamics deserves future studies to unravel the detailed thinning and rupture mechanism. In combination with foam stability measurements, these insights are expected to be of high relevance for technological applications of foam systems.

Acknowledgement

We would like to thank Zohreh Ghane for her help with the preliminary screening experiments of the system. We would also like to thank Nouryon (formerly AkzoNobel Specialty Chemicals) for providing the nanoparticle dispersions. Furthermore, we acknowledge the financial support provided by the German Helmholtz Association.

References

[1] D. Arab, A. Kantzas, S. L. Bryant, Nanoparticle stabilized oil in water emulsions: A critical review, Journal of Petroleum Science and Engineering 163 (2018) 217–242. doi:10.1016/j.petrol.2017.12.091.
URL https://doi.org/10.1016/j.petrol.2017.12.091

[2] B. Yuan, X. Jiang, Y. Chen, Q. Guo, K. Wang, X. Meng, Z. Huang, X. Wen, Metastatic cancer cell and tissue-specific fluorescence imaging using a new dna aptamer developed by cell-selex, Talanta 170 (2017) 56–62. doi:https://doi.org/10.1016/j.talanta.2017.03.094.
URL https://www.sciencedirect.com/science/article/pii/S0039914017304071

[3] C. C. Dewitt, Froth flotation concentration, Industrial and Engineering Chemistry 32 (5) (1940) 652–658. doi:10.1021/ie50365a014.

[4] B. J. Park, D. Lee, Particles at fluid–fluid interfaces: From single-particle behavior to hierarchical assembly of materials, MRS Bulletin 39 (12) (2014) 1089–1098. doi:10.1557/mrs.2014.253.
URL https://doi.org/10.1557/mrs.2014.253

[5] J. Frelichowska, M.-A. Bolzinger, J.-P. Valour, H. Mouaziz, J. Pelletier, Y. Chevalier, Pickering w/o emulsions: drug release and topical delivery, International journal of pharmaceutics 368 (1-2) (2009) 7–15.

[6] E. Dickinson, Food emulsions and foams: Stabilization by particles, Current Opinion in Colloid & Interface Science 15 (1) (2010) 40–49. doi:https://doi.org/10.1016/j.cocis.2009.11.001.
URL https://www.sciencedirect.com/science/article/pii/S1359029409001010

[7] A. A. Umar, I. B. M. Saaid, A. A. Sulaimon, R. B. M. Pilus, A review of petroleum emulsions and recent progress on water-in-crude oil emulsions stabilized by natural surfactants and solids, Journal of Petroleum Science and Engineering 165 (September 2017) (2018) 673–690. doi:10.1016/j.petrol.2018.03.014.
URL https://doi.org/10.1016/j.petrol.2018.03.014

[8] S. Kumar, V. K. Aswal, J. Kohlbrecher, Size-dependent interaction of silica nanoparticles with different surfactants in aqueous solution, Langmuir 28 (25) (2012) 9288–9297. doi:10.1021/la3019056.

[9] M. Eftekhari, K. Schwarzenberger, A. Javadi, K. Eckert, The influence of negatively charged silica nanoparticles on the surface properties of anionic surfactants: electrostatic repulsion or the effect of ionic strength?, Physical Chemistry Chemical Physics 22 (4) (2020) 2238–2248. doi:10.1039/C9CP05475H.
URL http://dx.doi.org/10.1039/C9CP05475H

[10] F. Ravera, M. Ferrari, L. Liggieri, G. Loglio, E. Santini, A. Zanobini, Liquid-liquid interfacial properties of mixed nanoparticle-surfactant systems, Colloids and Surfaces A: Physicochemical and Engineering Aspects 323 (1-3) (2008) 99–108. doi:10.1016/j.colsurfa.2007.10.017.

[11] S. M. Kirby, S. L. Anna, L. M. Walker, Effect of surfactant tail length and ionic strength on the interfacial properties of nanoparticle-surfactant complexes, Soft Matter 14 (1) (2017) 112–123. doi:10.1039/c7sm01806a.

[12] Q. Lan, F. Yang, S. Zhang, S. Liu, J. Xu, D. Sun, Synergistic effect of silica nanoparticle and cetyltrimethyl ammonium bromide on the stabilization of O/W emulsions, Colloids and Surfaces A: Physicochemical and Engineering Aspects 302 (1-3) (2007) 126–135. doi:10.1016/j.colsurfa.2007.02.010.

[13] B. a. Noskov, P. a. Yazhgur, L. Liggieri, S. Y. Lin, G. Loglio, R. Miller, F. Ravera, Dilational rheology of spread and adsorbed layers of silica nanoparticles at the liquid-gas interface, Colloid Journal 76 (2) (2014) 127–138. doi:10.1134/S1061933X14020057.

[14] L. Liggieri, E. Santini, E. Guzmán, A. Maestro, F. Ravera, Wide-frequency dilational rheology investigation of mixed silica nanoparticle-CTAB interfacial layers, Soft Matter 7 (17) (2011) 7699–7709. doi:10.1039/c1sm05257h.

[15] N. R. Biswal, N. Rangera, J. K. Singh, Effect of Different Surfactants on the Interfacial Behavior of the n-Hexane-Water System in the Presence of Silica Nanoparticles, Journal of Physical Chemistry B 120 (29) (2016) 7265–7274. doi:10.1021/acs.jpcb.6b03763.

[16] A. Maestro, E. Rio, W. Drenckhan, D. Langevin, A. Salonen, Foams stabilised by mixtures of nanoparticles and oppositely charged surfactants: Relationship between bubble shrinkage and foam coarsening, Soft Matter 10 (36) (2014) 6975–6983. doi:10.1039/c4sm00047a.
URL http://dx.doi.org/10.1039/C4SM00047A

[17] E. H. Lucassen-Reynders, D. T. Wasan, Interfacial Viscoelasticity in Emulsions and Foams, Food. Struct. 12 (1) (1993) 1–12.

[18] V. Ulaganathan, M. Krzan, M. Lotfi, S. S. Dukhin, V. I. Kovalchuk, A. Javadi, D. Z. Gunes, C. Gehin-Delval, K. Malysa, R. Miller, Influence of β-lactoglobulin and its surfactant mixtures on velocity of the rising bubbles, Colloids and Surfaces A: Physicochemical and Engineering Aspects 460 (2014) 361–368. doi:10.1016/j.colsurfa.2014.04.041.
URL http://dx.doi.org/10.1016/j.colsurfa.2014.04.041

[19] B. P. Binks, S. O. Lumsdon, Influence of particle wettability on the type and stability of surfactant-free emulsions, Langmuir 16 (23) (2000) 8622–8631. doi:10.1021/la000189s.

[20] E. Karpushkin, Rheology: Principles, applications and environmental impacts, in: Rheology: Principles, Applications and Environmental Impacts, 2015, pp. 1–254.

[21] M. S. Bhamla, C. E. Giacomin, C. Balemans, G. G. Fuller, Influence of interfacial rheology on drainage from curved surfaces, Soft Matter 10 (36) (2014) 6917–6925.

[22] H. Vatanparast, A. Javadi, A. Bahramian, Silica nanoparticles cationic surfactants interaction in water-oil system, Colloids and Surfaces A: Physicochemical and Engineering Aspects 521 (2017) 221–230. doi:10.1016/j.colsurfa.2016.10.004.

URL http://dx.doi.org/10.1016/j.colsurfa.2016.10.004

[23] S. Razavi, K. D. Cao, B. Lin, K. Y. C. Lee, R. S. Tu, I. Kretzschmar, Collapse of Particle-Laden Interfaces under Compression: Buckling vs Particle Expulsion, Langmuir 31 (28) (2015) 7764–7775. doi:10.1021/acs.langmuir.5b01652.

[24] L. K. Shrestha, E. Saito, R. G. Shrestha, H. Kato, Y. Takase, K. Aramaki, Foam stabilized by dispersed surfactant solid and lamellar liquid crystal in aqueous systems of diglycerol fatty acid esters, Colloids and Surfaces A: Physicochemical and Engineering Aspects 293 (1) (2007) 262–271. doi:https://doi.org/10.1016/j.colsurfa.2006.07.054.
URL https://www.sciencedirect.com/science/article/pii/S092777570600570X

[25] L. R. Arriaga, W. Drenckhan, A. Salonen, J. A. Rodrigues, R. Iniguez-Palomares, E. Rio, D. Langevin, On the long-term stability of foams stabilised by mixtures of nano-particles and oppositely charged short chain surfactants, Soft Matter 8 (43) (2012) 11085–11097.

[26] K. Velikov, F. Durst, O. Velev, Direct observation of the dynamics of latex particles confined inside thinning water- air films, Langmuir 14 (5) (1998) 1148–1155.

[27] L. Wang, D. Sharp, J. Masliyah, Z. Xu, Measurement of interactions between solid particles, liquid droplets, and/or gas bubbles in a liquid using an integrated thin film drainage apparatus, Langmuir 29 (11) (2013) 3594–3603.

[28] F. Ravera, E. Santini, G. Loglio, M. Ferrari, L. Liggieri, Effect of nanoparticles on the interfacial properties of liquid/liquid and liquid/air surface layers, Journal of Physical Chemistry B 110 (39) (2006) 19543–19551. doi:10.1021/jp0636468.

[29] J. H. Clint, S. E. Taylor, Particle size and interparticle forces of overbased detergents: A Langmuir trough study, Colloids and Surfaces 65 (1) (1992) 61–67. doi:10.1016/0166-6622(92)80175-2.

[30] L. A. Pugnaloni, R. Ettelaie, E. Dickinson, Brownian dynamics simulation of adsorbed layers of interacting particles subjected to large extensional deformation, Journal of colloid and interface science 287 (2) (2005) 401–414. doi:10.1016/j.jcis.2005.02.024.

[31] R. Aveyard, J. H. Clint, D. Nees, N. Quirke, Structure and collapse of particle monolayers under lateral pressure at the octane/aqueous surfactant solution interface, Langmuir 16 (23) (2000) 8820–8828. doi:10.1021/la000060i.

[32] A. Maestro, E. Guzmán, E. Santini, F. Ravera, L. Liggieri, F. Ortega, R. G. Rubio, Wettability of silica nanoparticle-surfactant nanocomposite interfacial layers, Soft Matter 8 (3) (2012) 837–843. doi:10.1039/c1sm06421e.

[33] M. Eftekhari, K. Schwarzenberger, S. Heitkam, A. Javadi, A. Bashkatov, S. Ata, K. Eckert, Interfacial behavior of particle-laden bubbles under asymmetric shear flow, Langmuir 37 (45) (2021) 13244–13254.

[34] S. A. Zholob, A. V. Makievski, R. Miller, V. B. Fainerman, Optimisation of calculation methods for determination of surface tensions by drop profile analysis tensiometry, Advances in Colloid and Interface Science 134-135 (2007) 322–329. doi:10.1016/j.cis.2007.04.011.

[35] D. Exerowa, P. M. Kruglyakov, Foam and foam films: theory, experiment, application, Elsevier, 1997.

[36] S. I. Karakashev, E. D. Manev, Hydrodynamics of thin liquid films: Retrospective and perspectives, Advances in colloid and interface science 222 (2015) 398–412.

[37] S. I. Karakashev, E. D. Manev, Correlation in the properties of aqueous single films and foam containing a nonionic surfactant and organic/inorganic electrolytes, Journal of Colloid and Interface Science 259 (1) (2003) 171–179. doi:https://doi.org/10.1016/S0021-9797(02)00189-3.
URL https://www.sciencedirect.com/science/article/pii/S0021979702001893

[38] R. Atkin, V. S. Craig, E. J. Wanless, S. Biggs, Mechanism of cationic surfactant adsorption at the solid-aqueous interface, Advances in Colloid and Interface Science 103 (3) (2003) 219–304. doi:10.1016/S0001-8686(03)00002-2.

[39] W. Wang, B. Gu, L. Liang, W. A. Hamilton, Adsorption and structural arrangement of cetyltrimethylammonium cations at the silica nanoparticle-water interface, Journal of Physical Chemistry B 108 (45) (2004) 17477–17483. doi:10.1021/jp048325f.

[40] J. Eastoe, S. Nave, A. Downer, A. Paul, A. Rankin, K. Tribe, J. Penfold, Adsorption of ionic surfactants at the air- solution interface, Langmuir 16 (10) (2000) 4511–4518.

[41] T. S. Horozov, Foams and foam films stabilised by solid particles, Current Opinion in Colloid and Interface Science 13 (3) (2008) 134–140. doi:10.1016/j.cocis.2007.11.009.

[42] E. S. Basheva, P. A. Kralchevsky, K. D. Danov, K. P. Ananthapadmanabhan, A. Lips, The colloid structural forces as a tool

for particle characterization and control of dispersion stability, Physical Chemistry Chemical Physics 9 (38) (2007) 5183–5198.

[43] I. Ahmad, F. Derkink, T. Boulogne, P. Bampoulis, H. J. Zandvliet, H. U. Khan, R. Jan, E. S. Kooij, Self-assembly and wetting properties of gold nanorod–ctab molecules on hopg, Beilstein journal of nanotechnology 10 (1) (2019) 696–705.

[44] F. Ravera, R. Miller, E. Santini, L. Liggieri, J. Krägel, Study of the monolayer structure and wettability properties of silica nanoparticles and CTAB using the Langmuir trough technique, Colloids and Surfaces A: Physicochemical and Engineering Aspects 382 (1-3) (2010) 186–191. doi:10.1016/j.colsurfa.2010.11.042.
URL http://dx.doi.org/10.1016/j.colsurfa.2010.11.042

[45] H. Wang, Y. Gong, W. Lu, B. Chen, Influence of nano-SiO 2 on dilational viscoelasticity of liquid/air interface of cetyltrimethyl ammonium bromide, Applied Surface Science 254 (11) (2008) 3380–3384. doi:10.1016/j.apsusc.2007.11.020.

[46] L. Jiang, S. Li, W. Yu, J. Wang, Q. Sun, Z. Li, Interfacial study on the interaction between hydrophobic nanoparticles and ionic surfactants, Colloids and Surfaces A: Physicochemical and Engineering Aspects 488 (2016) 20–27. doi:10.1016/j.colsurfa.2015.10.007.
URL http://dx.doi.org/10.1016/j.colsurfa.2015.10.007

Experimental protocol

Fig. A.1a shows the protocol of surface area and interfacial tension variation over time for surface pressure calculations. Four cycles of large amplitude compression/expansion experiments were performed after the system reached equilibrium. The droplet surface area was gradually decreased and then increased back to the initial surface area. During this process, the change in interfacial tension was recorded. The corresponding surface pressure was evaluated as the difference between the equilibrium interfacial tension of the uncompressed system and the interfacial tension under compression ($\Pi = \gamma_{eq} - \gamma$) as a function of the normalized surface area (A/A_0).

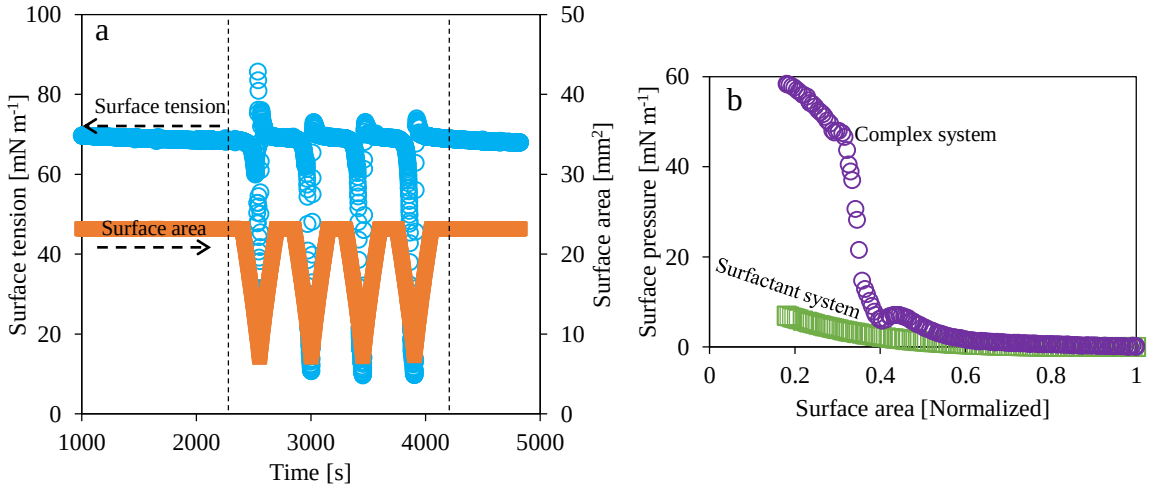

Figure A.1: **a**) Exemplary protocol of surface area and interfacial tension variation over time for surface pressure calculations. **b**) The calculated surface pressure isotherm from an exemplary compression cycle for surfactant and nanoparticle-surfactant complexes systems.

Surface tension of nanoparticle dispersion

Fig. A.2a and b show the surface tension of water with added silica nanoparticles for NP^9 and NP^{25}, respectively.

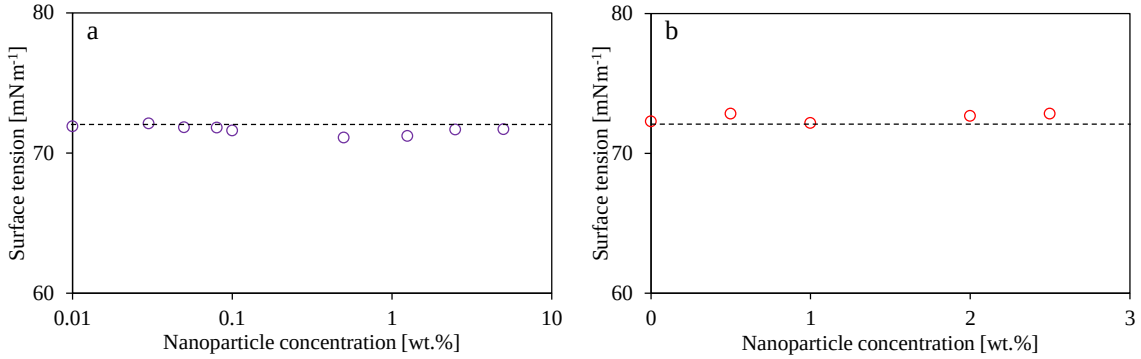

Figure A.2: Equilibrium surface tension of nanoparticles solution vs. nanoparticles concentration for **a)** 9 nm and **b)** 25 nm silica nanoparticles.

The effect of nanoparticle concentration of the surface tension of CTAB solution

Fig. A.3a and b show the effect of nanoparticle size on the surface tension of the CTAB solution at a constant nanoparticle concentration, a) 0.5 wt.% and b) 2.0 wt.%.

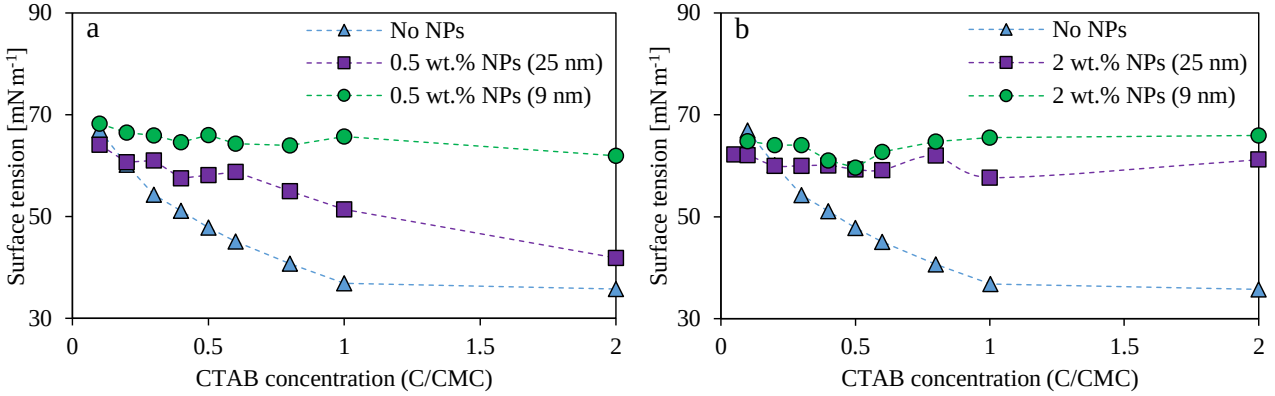

Figure A.3: The effect of nanoparticles size on the equilibrium surface tension of CTAB solutions at fixed concentration of nanoparticles **a**) 0.50 wt.% and **b**) 2.00 wt.%.

Zeta potential measurement at fixed ratio

Figure A.4 shows the zeta potential measurements of CTAB-Silica comlexes as a function of NPSCs concentration. The results show that the zeta potential remains nearly the same for different concentrations of NPSCs at the same ratio. Indeed, the zeta potential varies slightly with NPSC concentration due to the effects of ionic strength and pH changes caused by dilution, as shown in the figure.

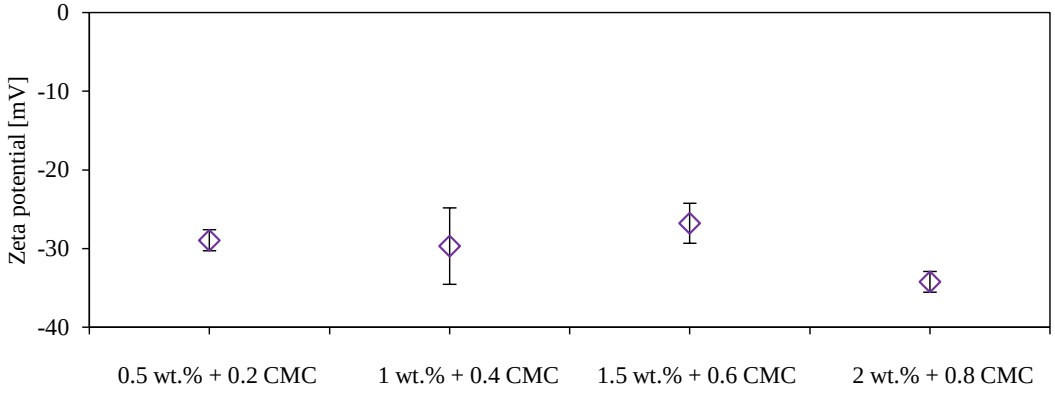

Figure A.4: Equilibrium surface tension of DTAB-silica nanoparticles of 9 nm vs. DTAB concentration.

Large amplitude compression/expansion experiments

Fig. A.5 compares the results of surface pressure measurements for different cycles of a) 1.00 wt.% + 0.2 CMC CTAB and b) 1.50 wt.% + 0.3 CMC CTAB. The surface pressure curve shifts to the right with each cycle, i.e.,

increased surface pressure is already obtained at higher surface areas (corresponding to lower compression), with a very large difference between the first cycle and the remaining cycles.

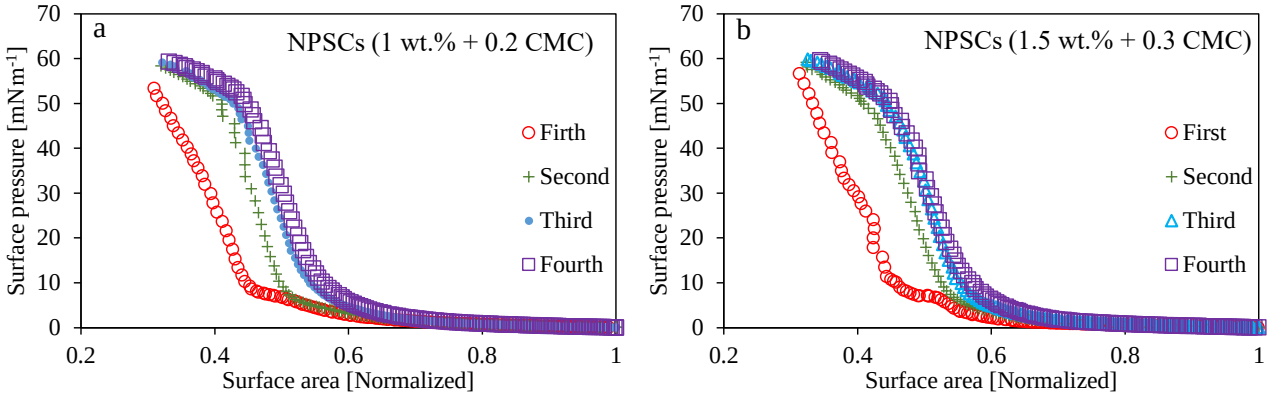

Figure A.5: Surface pressure as a function of surface area for different compression cycles i.e., first, second, third, and fourth. **a**) 1.00 wt.% + 0.2 CMC CTAB **b**) 1.50 wt.% + 0.3 CMC CTAB. The ratio of surfactant to nanoparticles was 0.036 nm^{-2} for all figures.

Fig. A.6 compares the results of surface pressure measurements for different cycles of a) 0.50 wt.% + 0.2 CMC

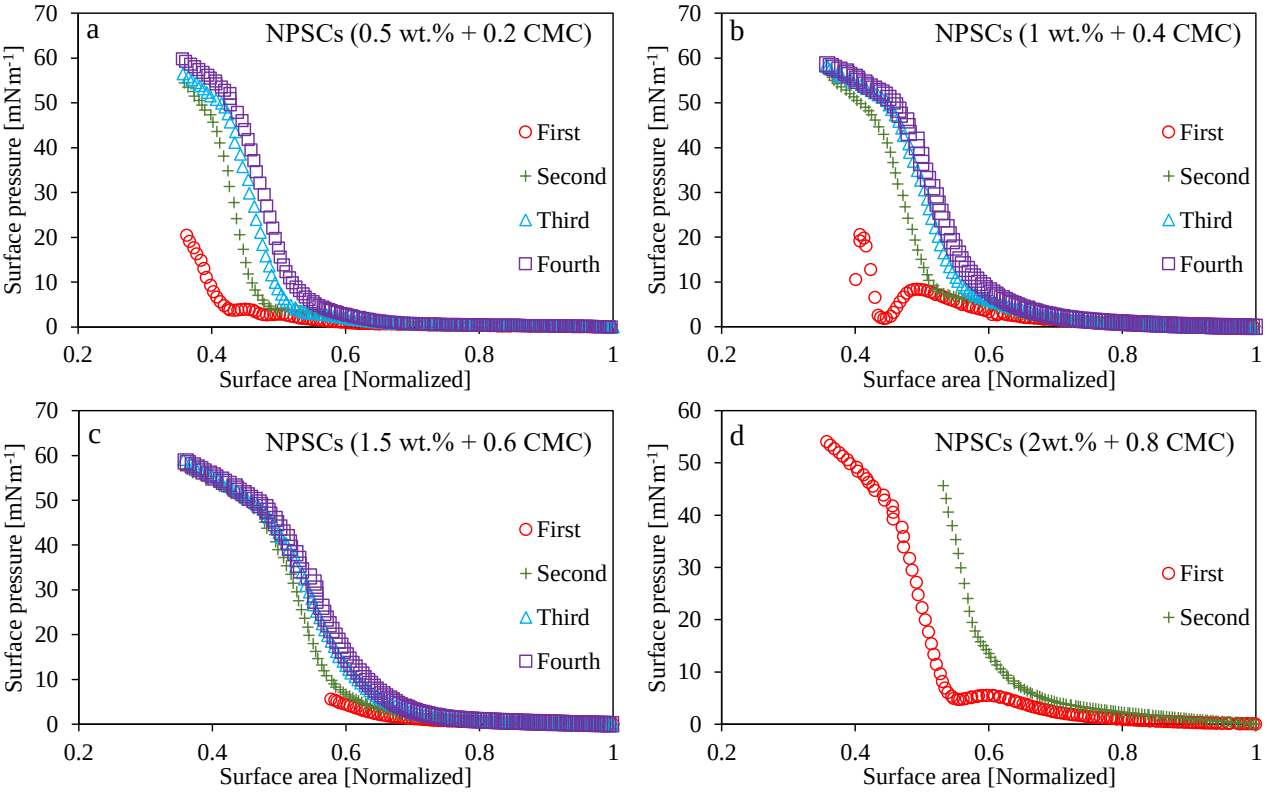

Figure A.6: Surface pressure as a function of surface area for different compression cycles i.e., first, second, third, and fourth for **a**) 0.50 wt.% + 0.2 CMC CTAB, **b**) 1.00 wt.% + 0.4 CMC CTAB, **c**) 1.5 wt.% + 0.6 CMC CTAB, and **d**) 2.00 wt.% + 0.8 CMC CTAB. The ratio of surfactant to nanoparticles was 0.072 nm^{-2} for all figures.

CTAB, b) 1.00 wt.% + 0.4 CMC CTAB, c) 1.50 wt.% + 0.6 CMC CTAB and b) 2.00 wt.% + 0.8 CMC CTAB, i.e., 0.072 nm^{-2}. Similar to the systems with surfactant to nanoparticle ratio of 0.036 nm^{-2}, the surface pressure curve shifts to the right with each cycle, i.e., increased surface pressure is already obtained at higher surface areas (corresponding to lower compression), with a very large difference between the first cycle and the remaining cycles.

Fig. A.7 and Fig. A.8 show surface pressure isotherms for different concentrations of nanoparticles and surfactants for different compression cycles at ratios 0.036 nm^{-2} and 0.072 nm^{-2}, respectively. Increasing NPSCs concentration results in a shift of the isotherm to higher surface areas. This means that the NPSCs concentration plays an important role in the response of the interfacial layers to compressive deformation. Since the hydrophobicity of the particles is the same within one figure, the effect can be attributed solely to the number of particles in the solution, which is supposed to affect the number of particles at the interface. This means that the (quasi-)equilibrium surface tension is not a sufficient indicator of the NPSCs behavior, as it is almost identical for all NPSCs in the uncompressed state (as shown in Fig. 5).

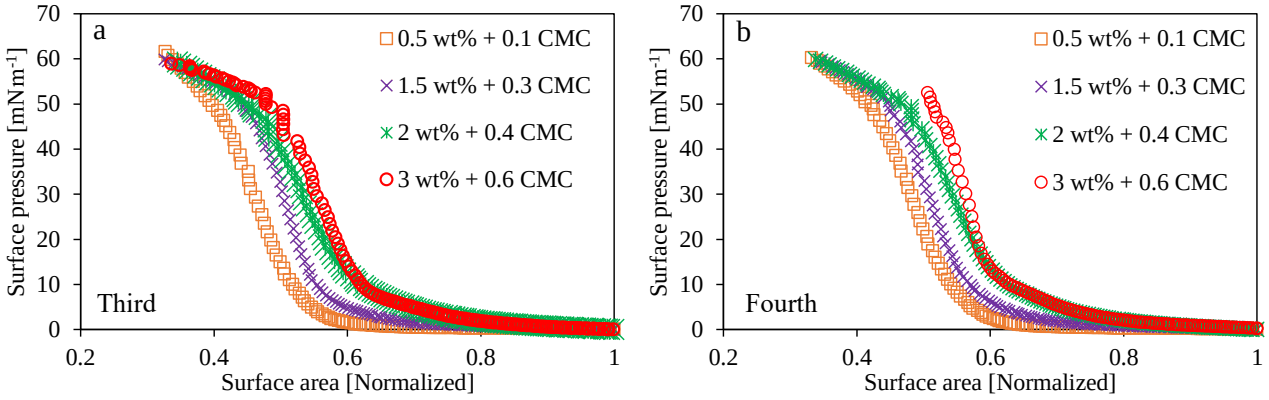

Figure A.7: Surface pressure as a function of surface area for different concentrations of nanoparticles and surfactants, at fixed ratio of 0.036 nm^{-2}. Each sub-figure represent a different compression/expansion cycle: **a**) third **b**) fourth.

Fig. A.9 plots the surface pressure isotherms for the two different hydrophobicity (surfactant/NP ratio 0.036 nm^{-2}, resp. 0.072 nm^{-2}). Increasing the hydrophobicity of the particles shifts the isotherm to the right, i.e. to higher surface areas, for 1.5 wt.% nanoparticles, for all compression cycles. However, a significant effect for the case of 0.5 wt.% was not observed.

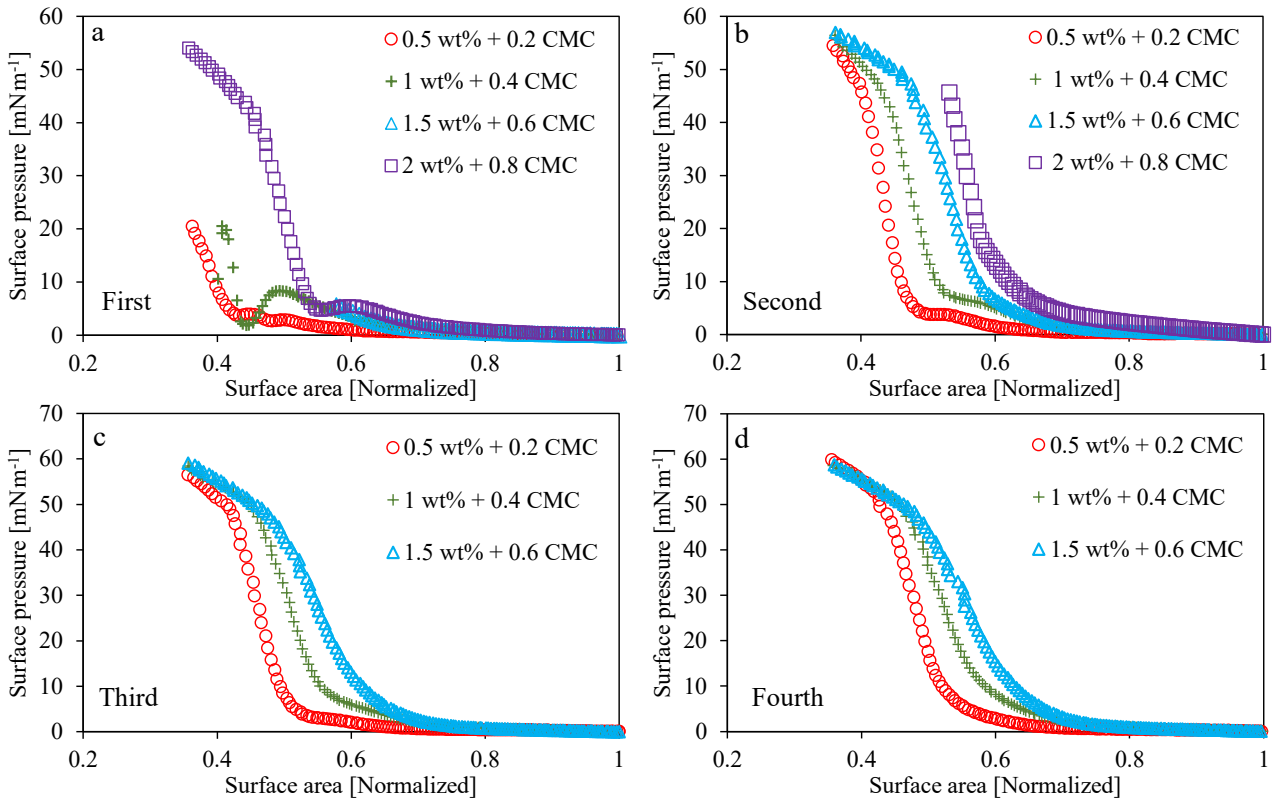

Figure A.8: Surface pressure as a function of surface area for different concentrations of nanoparticles and surfactants, but at fixed ratio of 0.072 nm^{-2}. Each sub-figure represent a different compression/expansion cycle: **a**) first **b**) second **c**) third **d**) fourth.

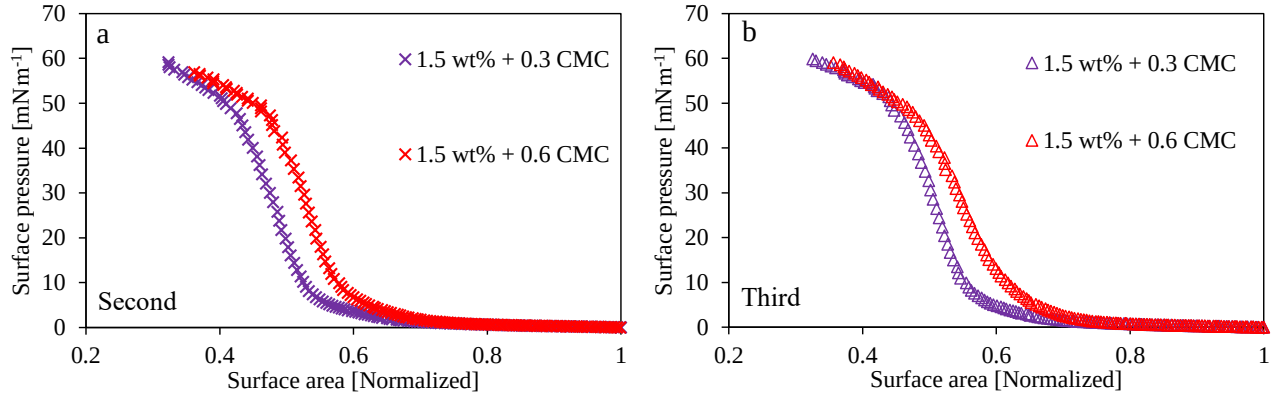

Figure A.9: Surface pressure vs. surface area for two different nanoparticle hydrophobicities at 1.5 wt.% NPSCs for **a**) second compression cycle and **b**) third compression cycle. The purple curve shows the surfactant/NP ratio 0.036 nm^{-2}, the red curve the surfactant/NP ratio 0.072 nm^{-2}.

Film stability with NPSCs

Figure A.10 shows the Type II liquid film during rupture. The rupture of Type II films is initiated by the formation of an irregular hole that gradually expands over several seconds. Type II liquid films have a

significantly longer life of approximately 6-7 seconds or more compared to Type I films, which rupture within microseconds. The slow expansion of the hole in Type II films is a remarkable indication of the significant surface viscosity imparted by the presence of NPSCs.

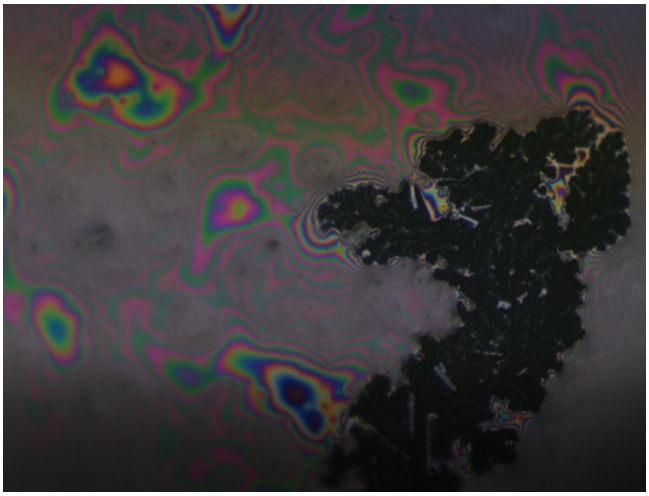

Figure A.10: Slowly expanding irregular rupture in liquid film of Type II.

Surface tension of DTAB-silica complexes

Figure A.11 shows the equilibrium surface tension values of NP^9-DTAB mixtures as a function of surfactant concentration. These preliminary experiments indicate a higher critical ratio for DTAB compared to CTAB, as evidenced by the nearly linear trend of DTAB complexes at higher ratios (Note that DTAB has much higher CMC than CTAB).

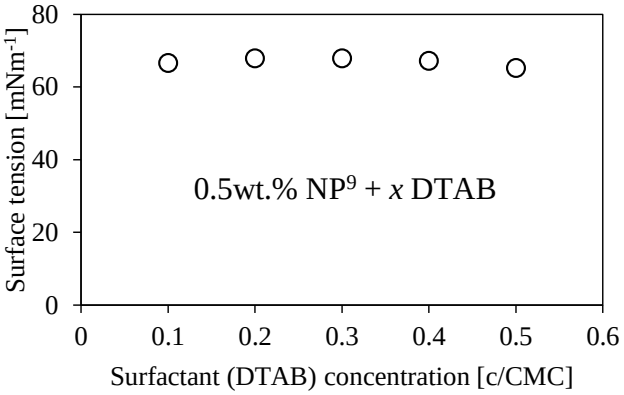

Figure A.11: Equilibrium surface tension of DTAB-silica nanoparticles of 9 nm vs. DTAB concentration.

Dyanmic surface tension measurement

To further illustrate the differences between NPSCs and NPSCs + free surfactant cases, the dynamic surface tension of 0.5 wt.% NP^{25} is measured with 0.2 and 0.8 CMC CTAB, see Fig. A.12. As can be seen, the dynamic

surface tension of the 0.8 CMC + 0.5 wt.% NP^{25} system is significantly different from that of the 0.2 CMC + 0.5 wt.% NP^{25} system and shows a very rapid surface tension decay (starting from near equilibrium values already from the beginning of the measurements). In contrast, the 0.2 CMC + 0.5 wt.% NP^{25} system, where no free surfactant is expected, shows very slow dynamics, i.e., the surface tension starts close to the surface tension of pure water and decreases over time to the (quasi-)equilibrium value.

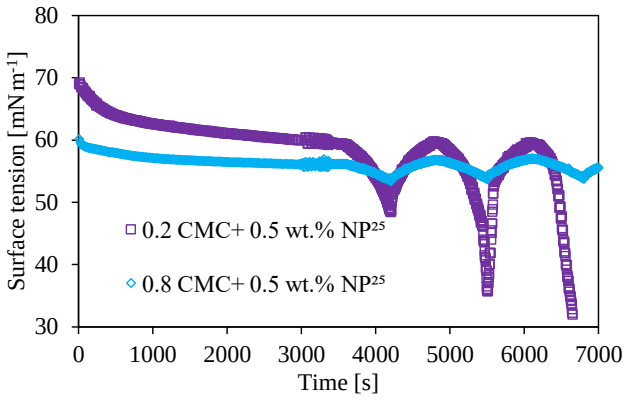

Figure A.12: Dynamic surface tension of 0.50 wt.% NP^{25} with 0.2 CMC and 0.8 CMC added CTAB.